How to cite: Angew. Chem. Int. Ed. **2021**, *60*, 8505–8509
International Edition: doi.org/10.1002/anie.202100006
German Edition: doi.org/10.1002/ange.202100006

Silver Clusters **Hot Paper**

Ultrafast Size Expansion and Turn-On Luminescence of Atomically Precise Silver Clusters by Hydrogen Sulfide

Wei-Miao He, Zhe Zhou, Zhen Han, Si Li, Zhan Zhou, Lu-Fang Ma, and Shuang-Quan Zang**

Abstract: *The formation of high-nuclearity silver(I) clusters remains elusive and their potential applications are still underdeveloped. Herein, we firstly prepared a chain-like thiolated* Ag^I *complex* $\{[Ag_{18}(S^tBu)_{10}(NO_3)_8(CH_3CN)_2(H_2O)_2]\cdot[Ag_{18}(S^tBu)_{10}(NO_3)_8(CH_3CN)_6]\}_n$ *(abbreviated as* $\mathbf{Ag_{18}}$*) in which two similar* $\mathbf{Ag_{18}}$ *clusters are assembled by* NO_3^- *anions. The solution containing* $\mathbf{Ag_{18}}$ *reacted with hydrogen sulfide with controlled concentration, promptly producing another identifiable and bright red-emitting high-nuclearity silver(I) cluster,* $Ag_{62}(S)_{13}(S^tBu)_{32}(NO_3)_4$ *(abbreviated as* $\mathbf{Ag_{62}}$*). We tracked the transformation using time-dependent electrospray ionization mass spectrometry (ESI-MS), UV/Vis absorption and photoluminescence spectra. Based on this cluster transformation, we further developed an ultra-sensitive turn-on sensor detecting* H_2S *gas with an ultrafast response time (30 s) at a low detection limit (0.13 ppm). This work opens a new way of understanding the growth of metal clusters and developing their luminescent sensing applications.*

Atomically precise metal clusters have attracted extraordinary attention attributed to their fascinating structures and wide applications in luminescence, sensors and biological antibacterial.[1] Silver clusters are considered as potential substitutes for luminescent gold clusters due to their excellent optical properties.[2] However, the formation mechanisms of high-nuclearity silver clusters have been a perplexing issue. The structural transformation and/or nuclear expansion, tailoring provide a unique platform to understand the formation process of metal clusters[3] by changing external conditions, such as peripheral ligand exchange,[4] doping of metal atoms[5] and the change of solvent molecules.[6] Although cluster transformation is an effective way to achieve the control of cluster structure and properties,[7] the process of metal cluster transformation is mostly slow, the nuclear size in clusters generally changes slightly[8] and can only happen under the unusual conditions including heating and excessive exchange ligands.[9] Now, the rapid and visualized metal cluster transformation under mild conditions is very scarcely observed.

Sulfur ions often template synthesis of high-nuclearity metal clusters,[10] and sulfur ions come from the fracture of carbon-sulfur bonds[11] or the additional sulfur components including the organosulfur compounds and the inorganic sulfur source.[12] However, to avoid the precipitate of metal-sulfide and get nanosize metal clusters, the slow release of sulfur ions from organosulfur compounds are preferably used during preparation.[13] Hydrogen sulfide, as a classical inorganic sulfur source, has been successfully used in the construction of small nuclear gold clusters or gold complexes,[14] are seldom used for directly preparing high-nuclearity silver clusters, probably because of the uncontrolled fast nucleation process in solution. Therefore, hydrogen sulfide-controlled high-nuclearity silver(I) cluster growth is still challenging, and no one has reported till now.

Here we report the first ultrafast size expansion of Ag^I cluster, from $\mathbf{Ag_{18}}$ (Supporting Information, Figure S1) without S^{2-} ions to $\mathbf{Ag_{62}}$ with 13 S^{2-} ions under room temperature by using hydrogen sulfide, which is accompanied with a high-contrast luminescence turn-on response (Figure 1). The prompt structural transformation was investigated by time-dependent mass spectrometry, UV/Vis absorption, photoluminescence spectra and crystal structure of the reactants ($\mathbf{Ag_{18}}$) and the products ($\mathbf{Ag_{62}}$). Based on this reaction, a new "turn-on" type photoluminescent probe can be developed for ultrasensitive and highly selective sensing hydrogen sulfide.

Compound $\{[Ag_{18}(C_4H_9S)_{10}(NO_3)_8(CH_3CN)_2(H_2O)_2]\cdot[Ag_{18}(C_4H_9S)_{10}(NO_3)_8(CH_3CN)_6]\}_n$ ($\mathbf{Ag_{18}}$) crystallizes in the triclinic space group $P\bar{1}$ and adopts a one-dimensional structure composed of Ag_{18} clusters bridged by NO_3^-. Of note, the adjacent clusters are distinct regarding to the protecting shell and are alternately arranged in the chain. One cluster contains eighteen Ag^I ions co-protected by ten $C_4H_9S^-$

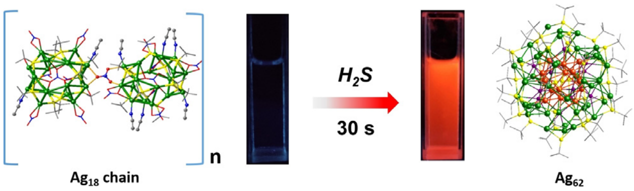

Figure 1. The structure of $\mathbf{Ag_{18}}$ and $\mathbf{Ag_{62}}$ respectively.[16] Color code: Ag, green and orange; S of S^tBu, yellow; S^{2-}, violet; O, red; N, blue; C, gray; H atoms are omitted for clarity. Inserted digital photos: the fast cluster transform is visualized by luminescent color: $\mathbf{Ag_{18}}$ (left, dark) and $\mathbf{Ag_{62}}$ (right, bright red) methanol solution by the irradiation of a 365 nm UV-lamp.

---

[*] W.-M. He, Z. Zhou, Z. Han, S. Li, Dr. Z. Zhou, Prof. S.-Q. Zang
Green Catalysis Center, and College of Chemistry, Zhengzhou University
Zhengzhou 450001 (China)
E-mail: zhouzhan@lynu.edu.cn
zangsqzg@zzu.edu.cn

Dr. Z. Zhou, Prof. L.-F. Ma
Henan Key Laboratory of Function-Oriented Porous Materials, College of Chemistry and Chemical Engineering, Luoyang Normal University
Luoyang 471934 (China)

Supporting information and the ORCID identification number(s) for the author(s) of this article can be found under: https://doi.org/10.1002/anie.202100006.

ligands, eight NO_3^-, two coordinated CH_3CN molecules and two H_2O molecules, while the neighboring one has six CH_3CN molecules in the ligand shell but no H_2O (Supporting Information, Figure S2). Both clusters share a macrocyclic ($Ag_{18}S_{10}$) cationic ($[Ag_{18}(C_4H_9S)_{10}]^{8+}$), which can be described as a three-layer sandwich structure: The interlayer is an Ag_8 ring, and two bilevel inverted Ag_5S_5 pentagrams located above and below the Ag_8 ring. Ag_5S_5 of two pentagonal rows are constructed alternately by Ag–S bonds. Finally, the bilayer inverted Ag_5S_5 pentagrams connect with the Ag_8 ring interlayer by Ag–Ag interactions and Ag–S bonds, thus creating a sandwich-shaped $Ag_{18}S_{10}$ cluster. Powder X-Ray Diffraction (PXRD) of **Ag$_{18}$** confirmed the phase purity of the as-synthesized product, which is used directly in the next step (Supporting Information, Figure S3).

The rational choice of sulfur source and controlled release of sulfur ion are the keys to prepare high-nuclearity metal clusters. After sodium hydrosulfide was carefully added as sulfur source into the **Ag$_{18}$** methanol solution, surprisingly, the colorless solution was rapidly (30 s) turned to red along with the appearance of red photoluminescence (Figure 1). Red block crystals were obtained after slowly evaporating methanol at room temperature. Single-crystal X-ray structural analysis revealed that the red crystal was composed of sixty-two silver(I) atoms, thirteen sulfur ions, thirty-two C_4H_9S and four nitrate ions with a formula as $Ag_{62}(S)_{13}(C_4H_9S)_{32}(NO_3)_4$ (**Ag$_{62}$**). Except for the different two coordinated NO_3^- and two NO_3^- counterions, the **Ag$_{62}$** was similar to the previously reported one prepared by using organic sulfur source at high temperature (65 °C) for 20 h.[11a] **Ag$_{62}$** nanocluster can be divided into an $Ag_{14}S_{13}$ core and an $Ag_{48}S_{32}$ shell connected by Ag–Ag and Ag–S bonds. (Supporting Information, Figure S4). $Ag_{14}S_{13}$ core can be regarded as a face-centered cube constructed by fourteen silver ions. One of the thirteen S^{2-} ions in $Ag_{14}S_{13}$ is located in the center of the cube bonding to six face-centered Ag atoms with the Ag–S distances in the range of 2.506–2.696 Å. The other twelve S^{2-} ions bridges three Ag atoms in the same facet. The $Ag_{48}S_{32}$ shell consists of forty-eight Ag atoms and thirty-two C_4H_9S assembled through Ag–Ag and Ag–S bonds. Two exposed Ag atoms in the shell are protected by two NO_3^-.

The chemical composition of **Ag$_{18}$** and **Ag$_{62}$** in solution was determined by high-resolution ESI-TOF-MS with the positive ion mode. As shown in Figure 2a, the mass curve of **Ag$_{18}$** had three main peaks at about 1459.97, 1544.92, and 1629.89 Da that was attributed to the $Ag_{16}(C_4H_9S)_8(NO_3)_6(CH_3CN)(CH_3OH)(H_2O)_2$ (abbreviated as **Ag$_{16}$**$^{2+}$, calcd = 1459.91), $Ag_{17}(C_4H_9S)_9(NO_3)_6$ $(CH_3OH)_2(H_2O)$ (abbreviated as **Ag$_{17}$**$^{2+}$, calcd = 1544.88), and $Ag_{18}(C_4H_9S)_{10}(NO_3)_6(H_2O)_3$ (abbreviated as **Ag$_{18}$**$^{2+}$, calcd = 1629.84), respectively. These three groups of peaks were ascribed to the dissociation of the bridged nitrate of chain-like **Ag$_{18}$**. As for the high-resolution ESI-TOF-MS of **Ag$_{62}$**, it was obvious that only one group of intense peaks at about 2489.55 Da within the *m*/*z* 1500–3500 Da range, which was perfectly aligned with the mass spectra of the four positively charged **Ag$_{62}$** (calcd = 2489.52) (Figure 2b).

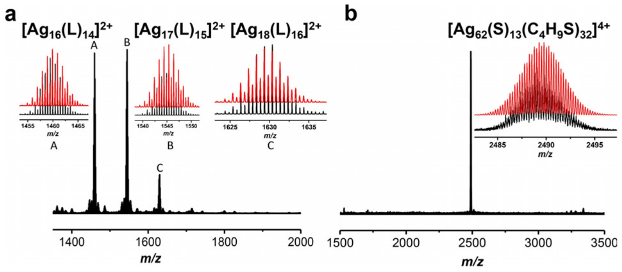

Figure 2. Mass spectra of **Ag$_{18}$** (a) and **Ag$_{62}$** (b), the measured (black trace) and simulated (red trace) isotopic distribution patterns of the corresponding the molecular ion peaks.

When the crystals are dissolved in methanol, the **Ag$_{62}$** solution portrays a bright red luminescence with the maximum emission band locates at near 603 nm (Supporting Information, Figure S5), while the **Ag$_{18}$** solution has no photoluminescence (Supporting Information, Figure S5) under the excitation wavelength of 392 nm. And the quantum yield of **Ag$_{62}$** solution was calculated to be 2.31 %. Meanwhile the UV/Vis spectrum of **Ag$_{62}$** divulges an absorption peak in the visible region (around 540 nm) whereas the **Ag$_{18}$** has no absorption peak under the same conditions (Supporting Information, Figure S6). The great difference observed between the emission and absorption of **Ag$_{62}$** and **Ag$_{18}$** will significantly display promising potentials in future detection.

The high-resolution mass spectrometry titration was performed to investigate the transformation mechanism from **Ag$_{18}$** to **Ag$_{62}$**. The titration mass spectrometry of **Ag$_{18}$** (1 $mg\,mL^{-1}$ in methanol) upon treatment with different concentrations of NaHS (0, 0.5, 1.0, 1.2, 1.5, 2.0 and 2.5 mM) for 5 min (Supporting Information, Figure S7). The peaks at about 1629.89, 1544.92, and 1459.97 Da (**Ag$_{18}$**$^{2+}$, **Ag$_{17}$**$^{2+}$, and **Ag$_{16}$**$^{2+}$) were gradually decreased with the increasing concentration of NaHS, while the peaks at about 2489.55 and 3340.10 Da (**Ag$_{62}$**$^{4+}$ and **Ag$_{62}$**$^{3+}$ Supporting Information, Figure S8) were formed with the 1.2 mM of NaHS and gradually enhanced with higher concentration of NaHS. Therefore, sodium hydrosulfide can react with **Ag$_{18}$** to produce **Ag$_{62}$** rapidly. To study the whole conversion process between **Ag$_{18}$** and **Ag$_{62}$**, the time-dependent high-resolution mass spectrometry was conducted (Figure 3). When adding

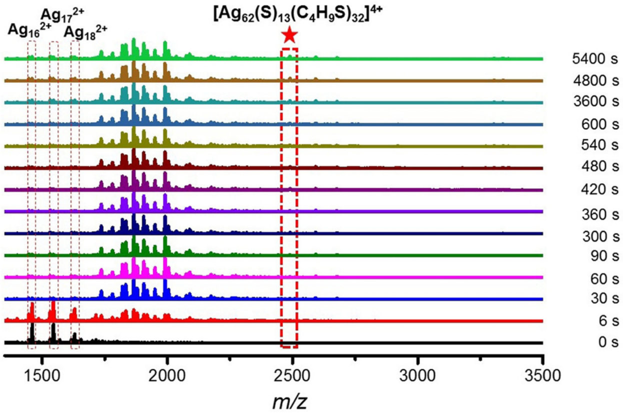

Figure 3. Time-dependent high-resolution mass spectrometry of **Ag$_{18}$** solution with the treatment of NaHS (1.2 mM).

NaHS (1.2 mM) to the **Ag_{18}** solution (1 mgmL^{-1}), the time-tracking mass spectrometry analysis found that the peaks of **Ag_{18}** (1459.97, 1544.92, and 1629.89 Da) were almost disappeared within 30 s, wihle some new peaks located at 1700–2300 Da were appeared, which was possible attributed to the formation of the small core silver clusters after the destruction of **Ag_{18}** by S^{2-}. Meanwhile, a new small peak at about 2489.55 Da (**$Ag_{62}{}^{4+}$**) was observed and growing as time goes on, which was proved that some of the above mentioned small core silver clusters are continued reassemble to the new silver cluster (**Ag_{62}**) by the stimulation of S^{2-}. Furthermore, we took videos to record the significant changes of photoluminescence and color from the **Ag_{18}** solution with or without the addition of sodium hydrosulfide. The strong red emission and light red color were rapidly observed after adding sodium hydrosulfide to the **Ag_{18}** solution (video 1 and video 2).

As we all know, H_2S is a kind of air pollutant, but play a crucial role in many physiological processes.[15] Therefore, it is urgent to develop a highly sensitive hydrogen sulfide probe. Based on the above experiments, it has been verified that the **Ag_{18}** solution is very sensitive to hydrogen sulfide, and it could be visually monitored by photoluminescence and UV/Vis spectrum, which provide good opportunities to quantitatively analyze hydrogen sulfide.

The photoluminescence kinetic spectrum was firstly conducted to investigate the response time between hydrogen sulfide and **Ag_{18}**, and the photoluminescence intensity of solution at 603 nm increased with the growing time and reached a plateau within 30 s (Supporting Information, Figure S9), which was consistent with the previous result of high-resolution mass spectrometry (Figure 3). When sodium hydrogen sulfide was added to **Ag_{18}** solution (0.1 mgmL^{-1}), the photoluminescence intensity increased gradually with increasing concentrations of NaHS from 0 to 150 μM (Figure 4a). The color of the solution immediately changed from colorless to pale yellow, accompanied with red photoluminescence under the excitation of a 365 nm UV light (Figure 4a, inset photo). Moreover, there was a good linear relationship between the photoluminescence intensity of **Ag_{18}** solution at 603 nm and the concentration of sodium hydrosulfide (Figure 4b). However, the addition of the other interferences including some ions (Ag^+, K^+, NH_4^+, Na^+, Cu^{2+}, Ba^{2+}, Mg^{2+}, Zn^{2+}, Cd^{2+}, Hg^{2+}, Co^{2+}, Cd^{2+}, Mn^{2+}, Gd^{3+}, Fe^{3+}, NO_3^-, NO_2^-, ClO_4^-, F^-, BF_4^-, PF_6^-, CH_3COO^-, SO_4^{2-}, HSO_3^-, and SO_3^{2-}), oxidizing substance (H_2O_2), some amino acids (GSH and Cys), and some common thiols (2-Propene-1-thiol, *tert*-butyl mercaptan, benzyl mercaptan, 4-*tert*- butylbenethiol, and [4-(*tert*-butyl)phenyl]methanethiol) did almost not change the photoluminescence in **Ag_{18}** solution (Figure 4c and d), which indicated that **Ag_{18}** could be used as a "turn-on" type of probe for selectively sensing hydrogen sulfide with excellent stability against various ions and highly oxidation and reduction substances. Moreover, it can also be found that the characteristic UV/Vis peak of **Ag_{62}** at 540 nm gradually increased upon adding the increasing concentration of NaHS from 0 to 150 μM (Figure 4e). Both photoluminescence and

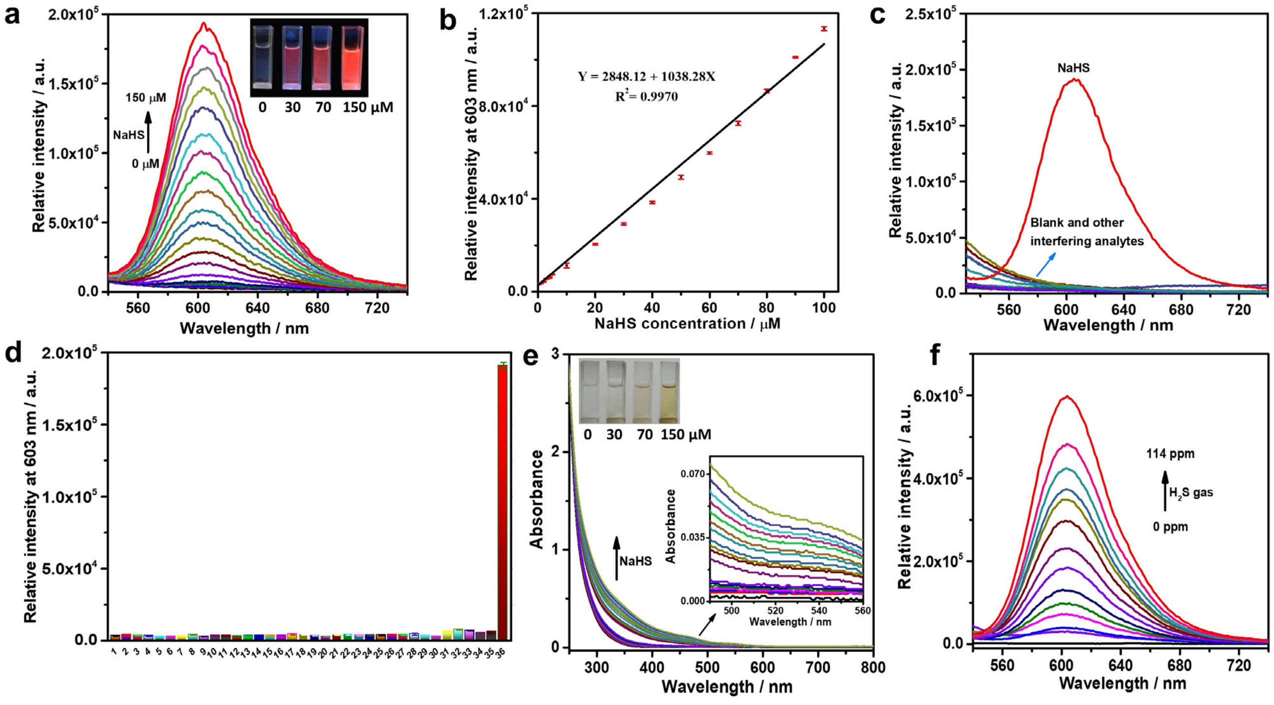

Figure 4. Photoluminescence diagram of NaHS titration (a), the linear relationship of NaHS titration (b), photoluminescence spectra of **Ag_{18}** solution before and after adding different substances (c), selectivity of **Ag_{18}** solution to NaHS (1 blank, 2 NH_4^+, 3 PF_6^-, 4 Na^+, 5 Ba^{2+}, 6 Cu^{2+}, 7 ClO_4^-, 8 F^-, 9 Mg^{2+}, 10 Ag^+, 11 NO_3^-, 12 Fe^{3+}, 13 H_2O_2, 14 Co^{2+}, 15 Mn^{2+}, 16 CH_3COO^-, 17 NO_2^-, 18 Cys, 19 GSH, 20 SO_3^{2-}, 21 HSO_3^-, 22 SO_4^{2-}, 23 BF_4^-, 24 HCO_3^-, 25 Cd^{2+}, 26 Zn^{2+}, 27 Gd^{3+}, 28 Hg^{2+}, 29 Cd^{2+}, 30 K^+, 31 2-Propene-1-thiol, 32 *tert*-Butyl Mercaptan, 33 BenzylMercaptan, 34 4-*tert*-Butylbenethiol, 35 [4-(*tert*-Butyl)phenyl]methanethiol and 36 HS^-, respectively) (d), UV/Vis spectra of **Ag_{18}** titrated by NaHS (e), photoluminescence diagram of H_2S gas (f).

UV/Vis spectra show that $\mathbf{Ag_{18}}$ could be able to serve as the fluorescent and colorimetric probe to detect hydrogen sulfide quantitatively.

To evaluate the performance of $\mathbf{Ag_{18}}$ in the real hydrogen sulfide gas, various amounts of H_2S gas were injected into the $\mathbf{Ag_{18}}$ solution ($0.1\ \text{mg}\,\text{mL}^{-1}$) carefully, and the photoluminescence and UV/Vis spectra were recorded. The photoluminescence relative intensity at 603 nm increased gradually with the increasing concentration (0–114 ppm) of H_2S gas, and showed a good linear relationship with a certain concentration range (from 24.4 to 105.8 ppm) of H_2S gas (Supporting Information, Figure S10). The LOD for H_2S gas was calculated as 0.13 ppm. Similar to that of sodium hydrosulfide, the UV/Vis peak at 540 nm increased with the increase of hydrogen sulfide gas (Supporting Information, Figure S11). Therefore, the transformation process between $\mathbf{Ag_{18}}$ to $\mathbf{Ag_{62}}$ can be used as a rapid, sensitive and selective probe for the real H_2S gas.

In summary, we prepared a new chain-like thiolated-silver(I) complex built from two alike $\mathbf{Ag_{18}}$ clusters assembled by nitrate. An ultrafast size expansion of silver clusters stimulated by hydrogen sulfide was observed and investigated by time-dependent ESI-MS, UV/Vis and photoluminescence spectra. The expansion process is accompanied by an effective “turn-on” luminescence phenomenon, which also supports quantitative NaHS detection as well as H_2S gas in a fast response time (30 s) with high sensitivity and a low hydrogen sulfide detection limit. This study significantly sheds light on cluster transformation and also greatly advances the promising applicability of atomically precise clusters in the future.

Acknowledgements

This work was supported by the National Natural Science Foundation of China (No. 92061201, 21825106, 21801227), the Program for Science & Technology Innovation Talents in Universities of Henan Province (164100510005), the Program for Innovative Research Team (in Science and Technology) in Universities of Henan Province (19IRTSTHN022) and Zhengzhou University, and the Scientific Research Fund of Henan Provincial Education Department (21A150003).

Conflict of interest

The authors declare no conflict of interest.

Keywords: cluster to cluster transformation · fluorescent probe · hydrogen sulfide · silver(I) clusters

---

[1] a) C. P. Joshi, M. S. Bootharaju, O. M. Bakr, *J. Phys. Chem. Lett.* **2015**, *6*, 3023–3035; b) R. Jin, C. Zeng, M. Zhou, Y. Chen, *Chem. Rev.* **2016**, *116*, 10346–10413; c) W. Kurashige, Y. Niihori, S. Sharma, Y. Negishi, *Coord. Chem. Rev.* **2016**, *320*, 238–250; d) I. Chakraborty, T. Pradeep, *Chem. Rev.* **2017**, *117*, 8208–8271; e) Q. Yao, T. Chen, X. Yuan, J. Xie, *Acc. Chem. Res.* **2018**, *51*, 1338–1348; f) X. Kang, M. Zhu, *Chem. Soc. Rev.* **2019**, *48*, 2422–2457; g) Z. Lei, Q. M. Wang, *Coord. Chem. Rev.* **2019**, *378*, 382–394; h) H. Schmidbaur, A. Schier, *Angew. Chem. Int. Ed.* **2015**, *54*, 746–784; *Angew. Chem.* **2015**, *127*, 756–797.

[2] a) S. Jin, S. Wang, Y. Song, M. Zhou, J. Zhong, A. Xia, Y. Pei, M. Chen, P. Li, M. Zhu, *J. Am. Chem. Soc.* **2014**, *136*, 15559–15565; b) R.-W. Huang, Y.-S. Wei, X.-Y. Dong, X.-H. Wu, C.-X. Du, S.-Q. Zang, T. C.-W. Mak, *Nat. Chem.* **2017**, *9*, 689–697; c) S.-X. Wang, X.-M. Meng, A. Das, T. Li, Y.-B. Song, T.-T. Cao, X.-Y. Zhu, M.-Z. Zhu, R.-C. Jin, *Angew. Chem. Int. Ed.* **2014**, *53*, 2376–2380; *Angew. Chem.* **2014**, *126*, 2408–2412; d) Z. Wang, H.-T. Sun, M. Kurmoo, Q.-Y. Liu, G.-L. Zhuang, Q.-Q. Zhao, X.-P. Wang, C.-H. Tung, D. Sun, *Chem. Sci.* **2019**, *10*, 4862–4867.

[3] a) Y. Li, M. J. Cowan, M. Zhou, T.-Y. Luo, Y. Song, H. Wang, N. L. Rosi, G. Mpourmakis, R. Jin, *J. Am. Chem. Soc.* **2020**, *142*, 20426–20433; b) S. C. Hau, P.-S. Cheng, T. C. Mak, *J. Am. Chem. Soc.* **2012**, *134*, 2922–2925; c) S. Li, X.-S. Du, B. Li, J.-Y. Wang, G.-P. Li, G.-G. Gao, S.-Q. Zang, *J. Am. Chem. Soc.* **2018**, *140*, 594–597; d) J. Yan, H.-F. Su, H. Yang, C. Hu, S. Malola, S.-C. Lin, B. K. Teo, H. Häkkinen, N. Zheng, *J. Am. Chem. Soc.* **2016**, *138*, 12751–12754; e) X. Kang, S. Jin, L. Xiong, X. Wei, M. Zhou, C. Qin, Y. Pei, S. Wang, M. Zhu, *Chem. Sci.* **2020**, *11*, 1691–1697; f) K. R. Krishnadas, A. Ghosh, A. Baksi, I. Chakraborty, G. Natarajan, T. Pradeep, *J. Am. Chem. Soc.* **2016**, *138*, 140–148.

[4] a) Y. Song, Y. Lv, M. Zhou, T.-Y. Luo, S. Zhao, N. L. Rosi, H. Yu, M. Zhu, R. Jin, *Nanoscale* **2018**, *10*, 12093–12099; b) S. Chen, L. Xiong, S. Wang, Z. Ma, S. Jin, H. Sheng, Y. Pei, M. Zhu, *J. Am. Chem. Soc.* **2016**, *138*, 10754–10757; c) Y. Wang, H. Su, C. Xu, G. Li, L. Gell, S. Lin, Z. Tang, H. Häkkinen, N. Zheng, *J. Am. Chem. Soc.* **2015**, *137*, 4324–4327; d) M. A. H. Muhammed, L. K. Cruz, A.-H. Emwas, A. M. ElZohry, B. Moosa, O. F. Mohammed, N. M. Khashab, *Angew. Chem. Int. Ed.* **2019**, *58*, 15665–15670; *Angew. Chem.* **2019**, *131*, 15812–15817; e) Z. Wang, H.-F. Su, C.-H. Tung, D. Sun, L.-S. Zheng, *Nat. Commun.* **2018**, *9*, 4407.

[5] a) R. Jin, K. Nobusada, *Nano Res.* **2014**, *7*, 285–300; b) S. Takano, S. Ito, T. Tsukuda, *J. Am. Chem. Soc.* **2019**, *141*, 15994–16002; c) X. Cai, G. Saranya, K. Shen, M. Chen, R. Si, W. Ding, Y. Zhu, *Angew. Chem. Int. Ed.* **2019**, *58*, 9964–9968; *Angew. Chem.* **2019**, *131*, 10069–10073; d) W. Zhang, S. Zhuang, L. Liao, H. Dong, N. Xia, J. Li, H. Deng, Z. Wu, *Inorg. Chem.* **2019**, *58*, 5388–5392; e) K. Zheng, V. Fung, X. Yuan, D. Jiang, J. Xie, *J. Am. Chem. Soc.* **2019**, *141*, 18977–18983.

[6] a) G.-T. Xu, L.-L. Wu, X.-Y. Chang, T. W. H. Ang, W.-Y. Wong, J.-S. Huang, C.-M. Che, *Angew. Chem. Int. Ed.* **2019**, *58*, 16297–16306; *Angew. Chem.* **2019**, *131*, 16443–16452; b) N. Xia, J. Yuan, L. Liao, W. Zhang, J. Li, H. Deng, J. Yang, Z. Wu, *J. Am. Chem. Soc.* **2020**, *142*, 12140–12145; c) S. F. Yuan, Z. J. Guan, W. D. Liu, Q. M. Wang, *Nat. Commun.* **2019**, *10*, 4032.

[7] a) Z. Qin, J. Zhang, C. Wan, S. Liu, H. Abroshan, R. Jin, G. Li, *Nat. Commun.* **2020**, *11*, 6019; b) X. Kang, L. Huang, W. Liu, L. Xiong, Y. Pei, Z. Sun, S. Wang, S. Wei, M. Zhu, *Chem. Sci.* **2019**, *10*, 8685–8693; c) S. Li, Z.-P. Yan, X.-L. Li, Y.-J. Kong, H.-Y. Li, G.-G. Gao, Y.-X. Zheng, S.-Q. Zang, *Adv. Sci.* **2020**, *7*, 2000738.

[8] a) S. Li, Z.-Y. Wang, G.-G. Gao, B. Li, P. Luo, Y.-J. Kong, H. Liu, S.-Q. Zang, *Angew. Chem. Int. Ed.* **2018**, *57*, 12775–12779; *Angew. Chem.* **2018**, *130*, 12957–12961; b) Y.-H. Li, R.-W. Huang, P. Luo, M. Cao, H. Xu, S.-Q. Zang, T. C.-W. Mak, *Sci. China Chem.* **2019**, *62*, 331–335; c) X.-H. Wu, P. Luo, Z. Wei, Y.-Y. Li, R.-W. Huang, X.-Y. Dong, K. Li, S.-Q. Zang, B.-Z. Tang, *Adv. Sci.* **2019**, *6*, 1801304; d) J.-Y. Wang, R.-W. Huang, Z. Wei, X.-J. Xi, X.-Y. Dong, S.-Q. Zang, *Chem. Eur. J.* **2019**, *25*, 3376–3381; e) X.-Y. Liu, Y. Yang, Z. Lei, Z.-J. Guan, Q.-M. Wang, *Chem. Commun.* **2016**, *52*, 8022–8025.

[9] a) C. Zeng, C. Liu, Y. Chen, N. L. Rosi, R. Jin, *J. Am. Chem. Soc.* **2014**, *136*, 11922–11925; b) A. Das, T. Li, G. Li, K. Nobusada, C. Zeng, N. L. Rosi, R. Jin, *Nanoscale* **2014**, *6*, 6458–6462; c) C. Zeng, T. Li, A. Das, N. L. Rosi, R. Jin, *J. Am. Chem. Soc.* **2013**, *135*, 10011–10013; d) C. Zeng, H. Qian, T. Li, G. Li, N. L. Rosi,

B. Yoon, R. N. Barnett, R. L. Whetten, U. Landman, R. Jin, *Angew. Chem. Int. Ed.* **2012**, *51*, 13114–13118; *Angew. Chem.* **2012**, *124*, 13291–13295.

[10] a) O. Fuhr, S. Dehnen, D. Fenske, *Chem. Soc. Rev.* **2013**, *42*, 1871–1906; b) M. L. Fu, I. Issac, D. Fenske, O. Fuhr, *Angew. Chem. Int. Ed.* **2010**, *49*, 6899–6903; *Angew. Chem.* **2010**, *122*, 7052–7056; c) Z. Wang, J. W. Liu, H. F. Su, Q. Q. Zhao, M. Kurmoo, X. P. Wang, C.-H. Tung, D. Sun, L.-S. Zheng, *J. Am. Chem. Soc.* **2019**, *141*, 17884–17890.

[11] a) G. Li, Z. Lei, Q.-M. Wang, *J. Am. Chem. Soc.* **2010**, *132*, 17678–17679; b) Z.-Y. Chen, D. Y. S. Tam, T. C.-W. Mak, *Chem. Commun.* **2016**, *52*, 6119–6122; c) Y.-M. Su, Z. Wang, S. Schein, C.-H. Tung, D. Sun, *Nat. Commun.* **2020**, *11*, 3316; d) Z.-A. Nan, Y. Xiao, X.-Y. Liu, T. Wang, X.-L. Cheng, Y. Yang, Z. Lei, Q.-M. Wang, *Chem. Commun.* **2019**, *55*, 6771–6774; e) S. Yang, J. Chai, H. Chong, Y. Song, H. Yu, M. Zhu, *Chem. Commun.* **2018**, *54*, 4314–4316.

[12] a) Z.-Y. Chen, D. Y. S. Tam, T. C.-W. Mak, *Nanoscale* **2017**, *9*, 8930–8937; b) J.-S. Yang, Z. Han, X.-Y. Dong, P. Luo, H.-L. Mo, S.-Q. Zang, *Angew. Chem. Int. Ed.* **2020**, *59*, 11898–11902; *Angew. Chem.* **2020**, *132*, 11996–12000.

[13] a) C. E. Anson, A. Eichhofer, I. Issac, D. Fenske, O. Fuhr, P. Sevillano, C. Persau, D. Stalke, J. Zhang, *Angew. Chem. Int. Ed.* **2008**, *47*, 1326–1331; *Angew. Chem.* **2008**, *120*, 1346–1351; b) S. Bestgen, O. Fuhr, B. Breitung, V. S. Kiran Chakravadhanula, G. Guthausen, F. Hennrich, W. Yu, M. M. Kappes, P. W. Roesky, D. Fenske, *Chem. Sci.* **2017**, *8*, 2235–2240.

[14] a) X. He, V. W.-W. Yam, *Coord. Chem. Rev.* **2011**, *255*, 2111–2123; b) L.-L. Yan, L.-Y. Yao, V. W.-W. Yam, *J. Am. Chem. Soc.* **2020**, *142*, 11560–11568; c) A. Chu, F. K.-W. Hau, L.-Y. Yao, V. W.-W. Yam, *ACS Mater. Lett.* **2019**, *1*, 277–284; d) C.-Y. Liu, X.-R. Wei, Y. Chen, H.-F. Wang, J.-F. Ge, Y.-J. Xu, Z.-G. Ren, P. Braunstein, J.-P. Lang, *Inorg. Chem.* **2019**, *58*, 3690–3697; e) L.-Y. Yao, T. K.-M. Lee, V. W.-W. Yam, *J. Am. Chem. Soc.* **2016**, *138*, 7260–7263; f) L.-Y. Yao, F. K.-W. Hau, V. W.-W. Yam, *J. Am. Chem. Soc.* **2014**, *136*, 10801–10806.

[15] a) L. Guo, M. Wang, D. Cao, *Small* **2018**, *14*, 1703822; b) Z. Wu, Z. Li, H. Li, M. Sun, S. Han, C. Cai, W. Shen, Y. Q. Fu, *ACS Appl. Mater. Interfaces* **2019**, *11*, 12761–12769; c) O. Yassine, O. Shekhah, A. H. Assen, Y. Belmabkhout, K. N. Salama, M. Eddaoudi, *Angew. Chem. Int. Ed.* **2016**, *55*, 15879–15883; *Angew. Chem.* **2016**, *128*, 16111–16115.

[16] Deposition Number(s) 2052080 and 2052137 (for $\mathbf{Ag_{18}}$ and $\mathbf{Ag_{62}}$, respectively) contain(s) the supplementary crystallographic data for this paper. These data are provided free of charge by the joint Cambridge Crystallographic Data Centre and Fachinformationszentrum Karlsruhe Access Structures service www.ccdc.cam.ac.uk/structures.

Manuscript received: January 1, 2021
Accepted manuscript online: January 23, 2021
Version of record online: March 3, 2021